ADVANCED FUNCTIONAL MATERIALS
www.afm-journal.de
www.MaterialsViews.com

High-Performance Olivine for Lithium Batteries: Effects of Ni/Co Doping on the Properties of $LiFe_\alpha Ni_\beta Co_\gamma PO_4$ Cathodes

*Gioele Pagot, Federico Bertasi, Graeme Nawn, Enrico Negro, Giorgio Carraro, Davide Barreca, Chiara Maccato, Stefano Polizzi, and Vito Di Noto**

New high voltage and high capacity storage systems are needed to sustain the increasing energy demand set by the portable electronics and automotive fields. Due to their good electrochemical performance, lithium-transition metal-phosphates ($LiMPO_4$) seem to be very attractive as cathode materials for lithium secondary batteries. Here the synthesis and the characterization of five high voltage cathodes for lithium batteries, based on lithium–iron, lithium–nickel, lithium–cobalt phosphates are described. The effect of differing degrees of cobalt and nickel doping on structure, morphology, and the electrochemical properties of the different materials is thoroughly studied. Transition metal atoms in these materials are found to be vicariant within the olivine crystal structure; however, the lattice parameters and cell volume can be modulated by varying the nickel/cobalt ratio during the synthesis. High performance battery prototypes in terms of voltage (>4.0 V), specific capacity (125 mAh g^{-1}), specific energy (560 mWh g^{-1}), and cyclic life (>150 cycles) are also demonstrated.

1. Introduction

The rate at which technology is advancing in areas such as portable electronics and the automotive field has generated an urgent need for improved performance in energy storage and conversion systems.[1–3] To date, the most promising battery systems are those based on lithium, owing to their high specific energy, high efficiency, and long lifespan.[4] In particular, lithium-ion batteries that incorporate lithium-cobalt-oxide ($LiCoO_2$) as the cathodic material currently dominate the market.[5] Over the years numerous attempts have been made to improve the properties of $LiCoO_2$ based cathodes. Although increases in performance were achieved (120–140 mAh g^{-1} at 3.0–4.0 V),[6] these materials suffered from low working potentials, high costs, and high toxicity. For these reasons there has always remained a broad scope for the development of cathodic materials.[7] One such development saw the introduction of lithium-transition metal-phosphates, $LiMPO_4$ (M = Ni, Fe, Co, or Mn). Due to their olivine structures, these materials are able to reversibly insert/de-insert lithium ions into the octahedral cavities created by the phosphate moieties. The 2D framework of crossed tunnels formed between LiO_6 edges enables the migration of lithium ions.[8] Reported in 1997 by Goodenough and co-workers, $LiFePO_4$, which is cheap, nontoxic, and environmentally friendly, was found to have a theoretic specific capacity of 170 mAh g^{-1} at ≈3.5 V versus Li. In addition, its stable nature allowed for good cyclability and long lifetimes.[9,10] Although $LiFePO_4$ found uses in the battery industry, in order to build batteries for automotive applications the working potentials were still too low. The substitution of nickel or cobalt for iron resulted in batteries with higher working potentials of ≈5.0 V. However, they suffered from very low practical specific capacities (≈50 mAh g^{-1}) owing to a low reversibility of about 50% and high decay during cycling. This limited the use of these materials for portable energy applications.[11–15] In general it was shown that high capacity cathodes suffered from low potential, giving low power, while high potential cathodic materials suffered from low capacity or very short lifespans. Attention has since turned to lithium-mixed transition metal-phosphates: doping $LiFePO_4$ with different divalent metal ions, such as Co^{2+}, Ni^{2+}, or Mn^{2+}, resulted in better electrochemical performance compared to that of the pure lithium-iron-phosphate. By controlling the molar ratio of the transition metal ions, the working potential can be increased from 3.5 to 4.8 V. In addition, an increased capacity has been

G. Pagot, Dr. G. Nawn
Department of Chemistry
University of Padova
via F. Marzolo, 1-35131 Padova, Italy
Dr. F. Bertasi, Dr. E. Negro, Dr. G. Carraro,
Prof. C. Maccato, Prof. V. Di Noto
Department of Chemistry
University of Padova and INSTM
via F. Marzolo, 1-35131 Padova, Italy
E-mail: vito.dinoto@unipd.it
Dr. D. Barreca
CNR-IENI and INSTM, Department of Chemistry
University of Padova
via F. Marzolo, 1-35131 Padova, Italy
Prof. S. Polizzi
Department of Molecular Sciences and Nanosystems
and Centre for Electron Microscopy "G.Stevanato"
Università Ca' Foscari Venezia
Via Torino 155/B, 30172 Venezia-Mestre, Italy

DOI: 10.1002/adfm.201501167

© 2015 WILEY-VCH Verlag GmbH & Co. KGaA, Weinheim

achieved that ranges from 90 to 160 mAh g^{-1} (especially when cycled at low current rates), and the cycle lifespan has also been improved.[16–22]

This work introduces a new series of lithium-mixed transition metal (iron, nickel, and cobalt)-phosphates at various nickel/cobalt ratios. Despite the differences in the metal molar ratios, all compounds exhibit the same olivine structure, where iron, nickel, and cobalt are vicariant. The volume of the crystal cell is found to increase with the increasing presence of cobalt. In addition the capacity of the cathodic materials tested in battery devices is found to increase, reaching a maximum of 125 mAh g^{-1} (560 mWh g^{-1} of specific energy), cycling between 4.0 and 5.0 V.

2. Results and Discussion

2.1. Synthesis and Composition

Five materials are prepared by a high temperature solid state reaction (700 °C in air for 24 h), starting from carbonates or oxides of the target elements and the phosphate source (Li_2CO_3, $(NH_4)_2HPO_4$, Fe_2O_3, NiO, and $2CoCO_3 \cdot 2Co(OH)_2 \cdot nH_2O$). The synthesized lithium transition metal phosphates ("$LiFe_\alpha Ni_\beta Co_\gamma PO_4$") described in this paper are labeled LFNCP$_x$ with x ($\beta = \beta_0 - x$ and $\gamma = \gamma_0 + x$) describing the variation of the molar ratios of nickel and cobalt to PO_4 moieties from the zero sample (the sample of highest content of nickel with α_0, β_0, and γ_0). In LFNCP$_x$, α is kept constant at the value $\alpha \approx \alpha_0 \approx 0.38$. Further information on the synthesis and the nomenclature can be found in the Supporting Information.

The chemical composition of all samples is evaluated by inductively coupled plasma atomic emission spectroscopy (ICP-AES) (**Table 1**). The molar ratios of the metals in the products are found to be very close to the target ratios set by reagent stoichiometry. This indicates that the high temperature solid state synthesis employed in this investigation is a very versatile protocol for modulating the metal composition of lithium-transition metal-phosphates. Thermo gravimetric analysis (TGA) shows that all samples are stable in the temperature range 30–950 °C and that they are not hygroscopic in nature, as proved by no observable mass loss (Figure S1, Supporting Information). Both these attributes are important for safety and application reasons. X-Ray photoelectron spectroscopy (XPS) analyses reveal the presence of carbon, oxygen, lithium, iron, cobalt, nickel, and phosphorous. In addition, binding energies and spin orbit coupling calculated from each 2p photoelectron peak[23–25] (Figure S2, Supporting Information) show that the transition metals are all in the +2 oxidation state. These results indicate that the chemical state of the transition metals is not affected by varying stoichiometry between the different materials.

2.2. Structure

Powder X-ray diffraction (XRD) analysis is conducted in order to probe how the crystal structure evolves with changing nickel and cobalt content (**Figure 1**a). The XRD pattern for all samples corresponds to a highly ordered olivine structure, agreeing well with related lithium-transition metal-phosphates described in the literature.[27] An orthorhombic *Pbnm* (62) space group is adopted with the M^{2+} ions located at the center of MO_6 octahedra. The lithium ions are found to occupy the octahedral cavities formed by the tetrahedral phosphate groups. It is these cavities that empty and fill of lithium ions during the charging/discharging processes.[10] In order to elucidate the effect of varying molar ratios on the structure of the materials, peaks attributed to planes (020), (111), (002), and (131) are analyzed in greater details (Figure 1b–e). The sharpness and gradual increase in 2θ of all four peaks, with increasing nickel content, indicates that the materials consist of a single-phase solid structure. The structure is based on vicariant multitransition-metal ions coordinated by lithium phosphates, rather than a simple multiphase blend of the individual lithium metal phosphates ($LiFePO_4$, $LiCoPO_4$, and $LiNiPO_4$). If this was the case, the XRD pattern would likely result in broad coalesced signals composed of the individual peaks for each species that differ slightly in 2θ values.[21] The lattice parameters are calculated from the diffraction patterns using the Rietveld refinement method (Table 1). With an increasing cobalt presence, *a*, *b*, and *c* are all rising, resulting in a growth in the unit cell volume. This is likely as a result of the larger ionic radius of Co(II) in the octahedral coordination geometry over that of Ni(II) (0.745 vs 0.690 Å).[28] The regularity with which the unit cell volume increases on cobalt content provides further support that the $LiFePO_4$ solid state olivine structure has been successfully doped with a variety of Ni/Co levels (Figure S3, Supporting Information), proving that these materials are indeed based on a single phase solid olivine.[19] The larger unit cell volume exhibited by the higher cobalt content derivatives is expected to increase the "free"

Table 1. ICP-AES results and crystal lattice parameters of the olivines with *Pbnm* (62) space group.

Sample	ICP-AES results	Rietveld refinement				
		a [Å]	*b* [Å]	*c* [Å]	*V* [Å^3]	R_{wp}[a)] [%]
LFNCP$_{0.00}$	$Li_{1.030}Fe_{0.380}Ni_{0.692}Co_{0.080}(PO_4)_{1.000}$	4.691	10.058	5.869	276.896	7.3
LFNCP$_{0.12}$	$Li_{1.062}Fe_{0.390}Ni_{0.570}Co_{0.201}(PO_4)_{1.000}$	4.695	10.090	5.884	278.736	6.2
LFNCP$_{0.32}$	$Li_{1.000}Fe_{0.394}Ni_{0.375}Co_{0.394}(PO_4)_{1.000}$	4.702	10.124	5.900	280.861	5.1
LFNCP$_{0.50}$	$Li_{1.040}Fe_{0.381}Ni_{0.187}Co_{0.569}(PO_4)_{1.000}$	4.707	10.178	5.919	283.551	4.7
LFNCP$_{0.61}$	$Li_{1.009}Fe_{0.383}Ni_{0.081}Co_{0.694}(PO_4)_{1.000}$	4.710	10.183	5.923	284.056	4.5

a) R_{wp} is the weighted profile R-factor, a discrepancy index used as one of the Rietveld error indices; it is calculated as follow: $R^2_{wp} = \Sigma_i w_i(y_{C,i}-y_{O,i})^2/\Sigma_i w_i(y_{O,i})^2$ where w_i are the weights ($1/\sigma^2[y_{O,i}]$), y_i indicates the intensity values, C stands for the computed values, while O is used for the observed values.[26]

© 2015 WILEY-VCH Verlag GmbH & Co. KGaA, Weinheim

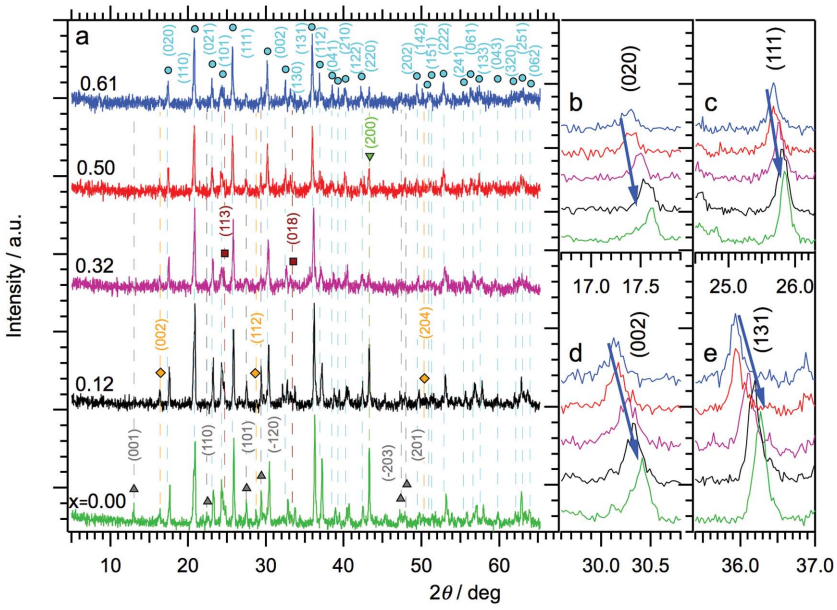

Figure 1. a) Powder XRD patterns of all LFNCP$_x$ samples; Miller indices are written above the peaks. Peaks of different phases are labeled with different markers (●$LiMPO_4$, ■Fe_2O_3, ▲$LiMP_2O_7$, ▼NiO, and ♦Li_3PO_4). b–e) Local magnification of (020), (111), (002), and (131) reflections.

volume within the solid and facilitate the migration of lithium ions during the charging/discharging process. A minor presence of some starting materials (NiO and Fe_2O_3) and byproducts ($LiMP_2O_7$ (M = Fe, Ni, and Co) and Li_3PO_4) is observed by XRD analysis, but accounts for just a few percent of the final materials' composition.

2.3. Morphology

Field emission-scanning electron microscopy (FE-SEM) images indicate that the morphology of all the samples is very similar, suggesting that composition does not significantly affect morphology (Figure S4, Supporting Information). A closer inspection of LFNCP$_{0.61}$ (**Figure 2**a,b) shows the presence of particles of two size distributions: small particles with a diameter of about 200 nm appear on the surface of larger particles of an average size of 1 µm. Representative transmission electron microscopy (TEM) images of LFNCP$_{0.61}$ are shown in Figure 2c (images of the other samples are shown in Figure S5, Supporting Information). The morphology of the samples is again found to be similar and the two dimensional particle size distributions are confirmed. The high crystallinity of LFNCP$_{0.61}$ is evidenced by high resolution transmission electron microscopy (HR-TEM) images, in which clear atomic planes can be observed (Figure 2d). In addition, the HR-TEM images show that these atomic planes are continuous in nature suggesting that the metals are able to coexist together in the same phase without making interruptions in the crystal structure. This provides further support that these materials exist as a single solid state phase consisting of vicariant multitransition-metal ions coordinated by lithium phosphates ligands within a 3D olivine structure. Interplanar distances in the reciprocal lattice are calculated by selected area diffraction analysis (SAD) (Figure 2e) which correspond to the reflections observed in the XRD analyses.

2.4. Vibrational Analysis

Vibrational Fourier transform spectroscopy in the mid-infrared (FT-MIR) and far-infrared (FT-FIR) regions allows for the identification of a variety of vibrational modes (**Figure 3**). Those of the phosphate groups (ν_1 and ν_3 involving the symmetric and antisymmetric stretching modes of P–O bonds, and ν_2 and ν_4 involving O–P–O symmetric and antisymmetric bending modes), diphosphate groups, lithium ion movements within phosphate cages and oxygen-[transition metal ions] bound species have been detected. A detailed analysis of the vibrational modes can be found in Table S1, Supporting Information. One notable feature of the IR spectra is the increasing degree to which the ν_4 band is split with increasing Ni(II) presence. The

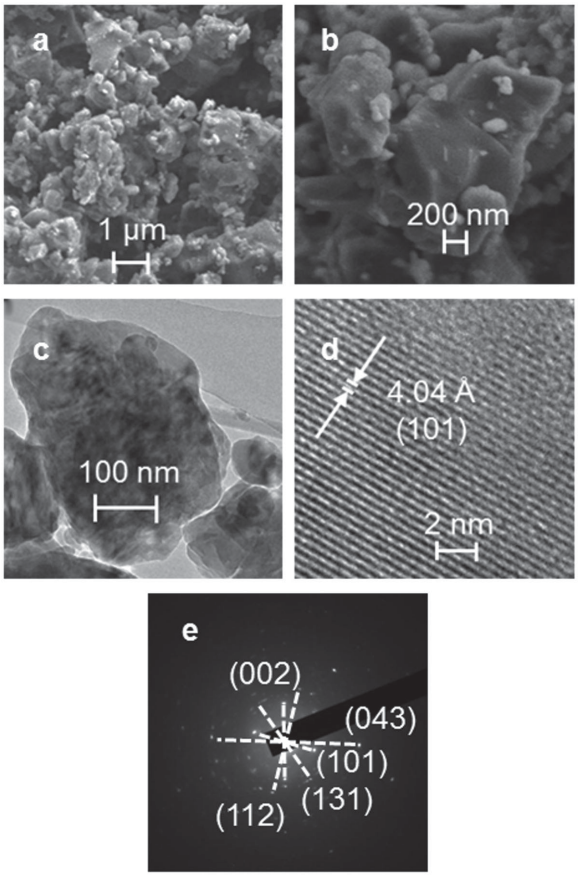

Figure 2. a,b) FE-SEM images of LFNCP$_{0.61}$. c) TEM image of LFNCP$_{0.61}$. d) HR-TEM image of LFNCP$_{0.61}$, with the observed interplanar distance and its corresponding Miller index. e) SAD pattern of LFNCP$_{0.61}$ with attributed Miller indices.

© 2015 WILEY-VCH Verlag GmbH & Co. KGaA, Weinheim

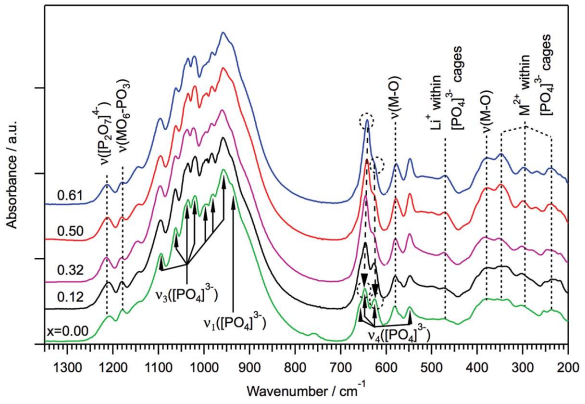

Figure 3. FT-MIR and FT-FIR spectra of LFNCP$_x$ samples with the assigned vibrational modes. The increased splitting of the ν_4 vibrational mode is highlighted.

magnitude of this splitting reflects the strength of interaction between the M(II) ion and the oxygen atoms from the associated phosphate groups.[29,30] This finding is in line with the higher second ionization potential for nickel with respect to cobalt (18.169 vs 17.084 eV).[31] This suggests that the derivatives with lower nickel content (higher cobalt content) may have a less rigid structure (higher structural elasticity) and can therefore more readily undergo the necessary expansions/contractions required in order to accommodate the lithium ions. Indeed, this increased ability to host lithium ions ("morphological elasticity") is reflected by an increase in capacity with increasing cobalt content (**Figure 4**d).

2.5. Electrochemical Characterizations

2.5.1. Cyclic Voltammetries

The cyclic voltammogram of LFNCP$_{0.61}$ is shown as a representative example (Figure 4a) with those of the other samples shown in Figure S6a, Supporting Information. One oxidation event is observed in the anodic region centered at ≈+4.9 V, while there appear to be three reduction events: one centered at ≈+4.8 V and a broader reduction event seemingly composed of two reduction processes occurring at ≈+4.0 V and ≈+4.2 V, respectively. The Ni(II/III) redox couple in $LiNiPO_4$ generally occurs at potentials in excess of +5.0 V. This exceeds the electrochemical stability window for the electrolyte used in this investigation and therefore, if it exists for these compounds, this redox couple is not observed.[32] Interestingly, the Fe(II/III) redox couple,

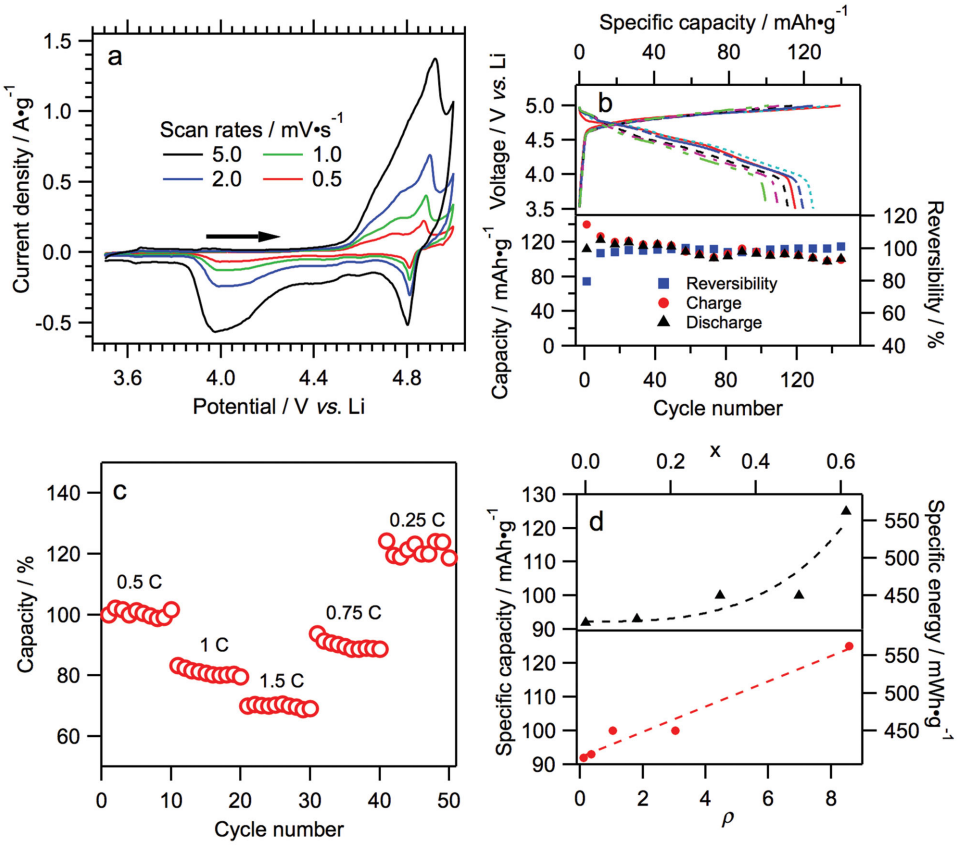

Figure 4. a) Cyclic Voltammetry (CV) curves of LFNCP$_{0.61}$ at various scan rates. b) Charge and discharge behaviors of the 1st (————), 5th (· · · · · · · · · ·), 10th (———— — — ————), 50th (— — — — — —), 100th (— · — · — · — · —), and 150th — · · — · · —) cycle and cycling stability of LFNCP$_{0.61}$. c) Discharge capacity of LFNCP$_{0.61}$ at different current densities (0.5 C is 78 mA g^{-1} and 100% of capacity is the capacity at the first cycle, 123 mAh g^{-1}). d) Maximum discharge capacity at different metal concentrations.

© 2015 WILEY-VCH Verlag GmbH & Co. KGaA, Weinheim

that usually appears about +3.5 V for similar systems, is not observed for these materials.[17,33] This suggests that either the Fe(II/III) redox couple is dramatically shifted to higher potentials or the iron electronic orbitals are not accessible because they are part of a larger electronic network that is delocalized throughout the mixed metal channels. In similar lithium-mixed metal-phosphates, the Co(II/III) redox couple is observed at ≈+4.8 V.[13,16,18] Although there are redox events observed in this region for $LFNCP_{0.61}$, there is an appreciable difference in magnitude between the forward and reverse waves occurring at ≈+4.9 and +4.8 V respectively. In addition, the presence of additional redox events at ≈+4.0 V suggests that these events are not purely cobalt centered. Indeed, confining the cyclic voltammetry (CV) experiment to scan only the high potential region (+4.5 to +5.0 V) results in a diminished oxidation signal over time, suggesting that the original species (before oxidation at +4.9 V) is not returned to following the reduction event at +4.8 V. This may suggest that the lithium ions are not re-inserted until after the reduction at ≈+4.0 V is reached. Only then can the system be oxidized again and stripped of Li^+. It is likely that the redox events are not localized to a specific ion center, but occur in a solid state electronic orbital originated from concurring contributions by all three metals, iron, nickel, and cobalt. For this reason, and according to the presence of a single phase vicariant distribution of multimetal coordination complexes suggested by XRD and HR-TEM analyses, these nonsymmetrical redox events could be assigned to an overall channel electrochemical behavior, modulated by the distribution of all the vicariant transition metal complexes present.

2.5.2. Battery Tests

The charge and discharge profile of $LFNCP_{0.61}$ over a range of 150 cycles is coherent with what is observed by CV (Figure 4b, top). The charge/discharge profiles of the other samples are shown in Figure S6b, Supporting Information. One plateau is observed for the charging (Li^+ de-insertion) process just as one reduction event is observed in the CV. Three plateaus are observed in the discharge profile corresponding to the three reduction events that are observed in the CV. After an initial activation period, lasting ≈10 cycles (Figure 4b, bottom), the reversibility and capacity of the system remain fairly constant for at least 150 cycles, highlighting the excellent service life of the target materials. The slight capacity fade over 150 cycles is likely caused by some electrolyte decomposition that starts at ≈+4.5 V (Figure S7, Supporting Information). The fade is, however, not large and these materials exhibit a good lifespan over the 150 cycle range. $LFNCP_{0.61}$ (which has the highest cobalt content) shows a maximum specific discharge capacity of 125 mAh g^{-1} at 0.5 C (78 mA g^{-1}), this corresponds to a specific energy of 560 mWh g^{-1} (both obtained referring to the cathodic active material weight). As the relative amount of cobalt decreases, the specific capacity does likewise, reaching a minimum value of 92 mAh g^{-1} for $LFNCP_{0.00}$ (Figure 4d). Due to the high working potentials of the presented cathodic materials, their specific energy is higher than those cathodic materials ($LiFePO_4$) currently used in lithium batteries.[19,21,33] In addition, at a low current rate, the capacity of the doped lithium-metal-phosphates is observed to increase (Figure 4c). Another crucial improvement is that the cycle life and capacity are shown to be better than cathodes based on $LiCoPO_4$.[11,16,18,22]

3. Conclusion

In summary, five different lithium-based cathode materials characterized by various nickel and cobalt contents are synthesized and extensively characterized. It is observed that different relative ratios of cobalt and nickel do not affect the morphology of the compounds, but play a crucial role in modulating the resulting electrochemical properties of the materials. Indeed, it is found that the material composition affects: (a) the structure elasticity of olivines and (b) the electronic density of states of insertion/de-insertion Li^+ ion channels. Specifically, the crystal cell volume increases with increasing cobalt presence. This is thought to facilitate the migration of lithium ions during the insertion and de-insertion processes of battery cycling. It is demonstrated that the material with the highest cobalt content shows the best performance in terms of rate capabilities, high working potentials (above 4.5 V), good capacities (125 mAh g^{-1}), and exceptional energy densities (560 mWh g^{-1}). These values are referred to the cathodic active material weight and not to the complete device, in order to highlight the material performance. As a whole, this study shows that transition metal doped $LiMPO_4$ are high performance materials for lithium secondary batteries. This new family of systems could address the current demands for improved energy storage and conversion technologies.

4. Experimental Section

Materials: Lithium metal, polyvinyl difluoride (PVDF), 1-methyl-2-pyrrolidone (99.5%, anhydrous), ethylene carbonate (99%, anhydrous), and dimethyl carbonate (>99%, anhydrous) are purchased from Sigma-Aldrich. Lithium carbonate (99%) is obtained from BDH, ammonium phosphate dibasic (99%) from Riedel-de Haën, iron(III) oxide from Baker, nickel(II) oxide (97%), and cobalt(II) carbonate (50.5% assay) from Carlo Erba, graphite (type SK6) from TIMCAL and lithium hexafluorophosphate (98%) from Acros. All materials are used as received.

$LFNCP_x$ Synthesis: Li_2CO_3 (1.00 g, 13.5 mmol), $(NH_4)_2HPO_4$ (3.57 g, 27.0 mmol), Fe_2O_3 (0.72 g, 4.5 mmol), NiO (1.21–1.01–0.68–0.34–0.14 g, 16.2–13.5–9.1–4.6–1.9 mmol), and $2CoCO_3{\cdot}2Co(OH)_2{\cdot}nH_2O$ (0.22–0.54–1.05–1.58–1.90 g, 1.9–4.6–9.0–13.5–16.3 mmol of Co^{2+}) are mixed in a planetary ball mill (2 h, 500 rpm). After the milling process, pellets of each sample are obtained by sintering the powders under a pressure of 4 tons. Each pellet is then put into a furnace at 700 °C in air for 24 h before being allowed to cool slowly. Finally, at the end of the pyrolysis, materials are ground again via planetary ball milling (2 h, 500 rpm).

Cathodic Mixtures for Electrochemical Tests: Sample powders were mixed with graphite (SK6) and PVDF in a ratio 4:15:1. PVDF is used as a plasticizer, while graphite is employed to improve the low electronic conductivity of the synthesized materials. The mixtures are suspended in 1-methyl-2-pyrrolidone producing an ink; for battery tests the inks are deposited and dried directly on nickelated stainless steel current collector tipically used in CR2032 type batteries. The loading of active material is ≈7 mg cm^{-2}. For the CV experiments the inks are deposited on a platinum wire (≈1.6 mg cm^{-2}). CV measurements are obtained using a three electrode configuration: samples inks as the working electrode and two pieces of lithium metal as the reference and the counter electrodes

© 2015 WILEY-VCH Verlag GmbH & Co. KGaA, Weinheim

(working electrodes were weighed before and after the ink deposition, in order to calculate the cathodic active mass); all electrodes are immersed in a 1 M $LiPF_6$ in EC/DMC 1:1 electrolytic solution. CV measurements are run at 20 °C, between 3.5 and 5.0 V, at scan rates of 5.0, 2.0, 1.0, and 0.5 mV s^{-1}. The electrolyte stability window is measured with a linear sweep voltammetry using, as working electrode, the same platinum wire used in the CV tests, and two pieces of lithium metal as the reference and the counter electrodes. Linear sweep voltammetry is performed at 20 °C, from 3.5 to 5.0 V, at a scan rate of 5.0 mV s^{-1}. Battery tests are performed assembling CR2032 coin cells with a lithium metal foil (13 mm of diameter) as the anode and 1 M $LiPF_6$ in EC/DMC 1:1 as the electrolytic solution. Battery testing is carried out by cycling between 3.5 and 5.0 V at a constant current of 100 μA for 150 cycles at room temperature.

Supporting Information

Supporting Information is available from the Wiley Online Library or from the author.

Acknowledgements

This study was funded by the strategic project MAESTRA of the University of Padova and Breton S.p.a. (Castello di Godego, Treviso). G.C., D.B., and C.M. kindly acknowledge the financial support from Padova University ex-60% 2012–2014 and Grant No. CPDR132937/13 (SOLLEONE).

Received: March 23, 2015
Revised: April 23, 2015
Published online: May 20, 2015

[1] M. Armand, J. M. Tarascon, *Nature* **2008**, *451*, 652.
[2] B. Dunn, H. Kamath, J. M. Tarascon, *Science* **2011**, *334*, 928.
[3] H. Chen, T. N. Cong, W. Yang, C. Tan, Y. Li, Y. Ding, *Prog. Natl. Acad. Sci. U.S.A.* **2009**, *19*, 291.
[4] B. Scrosati, J. Garche, *J. Power Sources* **2010**, *195*, 2419.
[5] K. Zaghib, A. Mauger, H. Groult, J. B. Goodenough, C. M. Julien, *Materials* **2013**, *6*, 1028.
[6] R. Koksbang, J. Barker, H. Shi, M. Y. Saïdi, *Solid State Ionics* **1996**, *84*, 1.
[7] K. Zaghib, J. Dubé, A. Dallaire, K. Galoustov, A. Guerfi, M. Ramanathan, A. Benmayza, J. Prakash, A. Mauger, C. M. Julien, *J. Power Sources* **2012**, *219*, 36.
[8] V. A. Streltsov, E. L. Belokoneva, V. G. Tsirelson, N. K. Hansen, *Acta Crystallogr., Sect. B: Struct. Sci.* **1993**, *B49*, 147.
[9] Y. Zhang, Q. Y. Huo, P. P. Du, L. Z. Wang, A. Q. Zhang, Y. H. Song, Y. Lv, G. Y. Li, *Synth. Met.* **2012**, *162*, 1315.
[10] A. K. Padhi, K. S. Nanjundaswamy, J. B. Goodenough, *J. Electrochem. Soc.* **1997**, *144*, 1188.
[11] N. N. Bramnik, K. G. Bramnik, T. Buhrmester, C. Baehtz, H. Ehrenberg, H. Fuess, *J. Solid State Electrochem.* **2004**, *8*, 558.
[12] M. Hu, X. Pang, Z. Zhou, *J. Power Sources* **2013**, *237*, 229.
[13] H. Li, Y. Wang, X. Yang, L. Liu, L. Chen, J. Wei, *Solid State Ionics* **2014**, *255*, 84.
[14] M. Minakshi, P. Singh, D. Appadoo, D. E. Martin, *Electrochim. Acta* **2011**, *56*, 4356.
[15] J. Wolfenstine, J. Allen, *J. Power Sources* **2005**, *142*, 389.
[16] D. W. Han, Y. M. Kang, R. Z. Yin, M. S. Song, H. S. Kwon, *Electrochem. Commun.* **2009**, *11*, 137.
[17] Q. Liu, Z. Liu, G. Xiao, S. Liao, *Ionics* **2013**, *19*, 445.
[18] J. F. Ni, Y. Han, J. Liu, H. Wang, L. Gao, *ECS Electrochem. Lett.* **2013**, *2*, A3.
[19] S. Novikova, S. Yaroslavtsev, V. Rusakov, T. Kulova, A. Skundin, A. Yaroslavtsev, *Electrochim. Acta* **2014**, *122*, 180.
[20] Y. K. Sun, S. M. Oh, H. K. Park, B. Scrosati, *Adv. Mater.* **2011**, *23*, 5050.
[21] Y. Zhang, C. S. Sun, Z. Zhou, *Electrochem. Commun.* **2009**, *11*, 1183.
[22] J. L. Allen, T. R. Jow, J. Wolfenstine, *J. Power Sources* **2011**, *196*, 8656.
[23] S. Cobo, J. Heidkamp, P. A. Jacques, J. Fize, V. Fourmond, L. Guetaz, B. Jousselme, V. Ivanova, H. Dau, S. Palacin, M. Fontecave, V. Artero, *Nat. Mater.* **2012**, *11*, 802.
[24] Y. Wang, D. J. Asunskis, P. M. A. Sherwood, *Surf. Sci. Spectra* **2002**, *9*, 91.
[25] M. Zhi, X. Chen, H. Finklea, I. Celik, N. Q. Wu, *J. Power Sources* **2008**, *183*, 485.
[26] B. H. Toby, *Powder Diffr.* **2006**, *21*, 67.
[27] C. O. Bjoerling, A. Westgren, *GFF* **1938**, *60*, 67.
[28] R. D. Shannon, *Acta Crystallogr., Sect. A: Cryst. Phys., Diffr., Theor. Gen. Crystallogr.* **1976**, *A32*, 751.
[29] O. García-Moreno, M. Alvarez-Vega, F. García-Alvarado, J. García-Jaca, J. M. Gallardo-Amores, M. L. Sanjuán, U. Amador, *Chem. Mater.* **2001**, *13*, 1570.
[30] A. A. Salah, P. Jozwiak, J. Garbarczyk, K. Benkhouja, K. Zaghib, F. Gendron, C. M. Julien, *J. Power Sources* **2005**, *140*, 370.
[31] W. M. Haynes, *CRC Handbook of Chemistry and Physics*, 93rd ed., Taylor & Francis, Boca Raton, FL **2012**.
[32] S. M. Rommel, N. Schall, C. Brünig, R. Weihrich, *Monatsh. Chem.* **2014**, *145*, 385.
[33] J. Liu, M. N. Banis, Q. Sun, A. Lushington, R. Li, T. K. Sham, X. Sun, *Adv. Mater.* **2014**, *26*, 6472.

© 2015 WILEY-VCH Verlag GmbH & Co. KGaA, Weinheim